





Article

Performance Analysis of Helical Milling and Drilling Operations While Machining Carbon Fiber-Reinforced Aluminum Laminates

Gururaj Bolar ¹, Anoop Aroor Dinesh ², Ashwin Polishetty ³, Raviraj Shetty ^{1,*}, Anupama Hiremath ^{1,*}
and V. L. Neelakantha ⁴

¹ Department of Mechanical & Industrial Engineering, Manipal Institute of Technology, Manipal Academy of Higher Education, Manipal 576104, India; gururaj.bolar@manipal.edu

² Department of Mechanical Engineering, National Institute of Technology Goa, Ponda 403401, India

³ School of Engineering, Computer and Mathematical Science, Auckland University of Technology, Auckland 1010, New Zealand; ashwin.polishetty@aut.ac.nz

⁴ Department of Mechanical Engineering, Mangalore Institute of Technology and Engineering, Moodbidri, Mangalore 574225, India

* Correspondence: rr.shetty@manipal.edu (R.S.); anupama.hiremath@manipal.edu (A.H.)

Abstract: Being a difficult-to-cut material, Fiber Metal Laminates (FML) often pose challenges during conventional drilling and require judicious selection of machining parameters to ensure defect-free laminates that can serve reliably during their service lifetime. Helical milling is a promising technique for producing good-quality holes and is preferred over conventional drilling. The paper compares conventional drilling with the helical milling technique for producing holes in carbon fiber-reinforced aluminum laminates. The effect of machining parameters, such as cutting speed and axial feed, on the magnitude of cutting force and the machining temperature during conventional drilling as well as helical milling is studied. It was observed that the thrust force produced during machining reduces considerably during helical milling in comparison to conventional drilling at a constant axial feed rate. The highest machining temperature recorded for helical milling was much lower in comparison to the highest machining temperature measured during conventional drilling. The machining temperatures recorded during helical milling were well below the glass transition temperature of the epoxy used in carbon fiber prepreg, hence protecting the prepreg from thermal degradation during the hole-making process. The surface roughness of the holes produced by both techniques is measured, and the surface morphology of the drilled holes is analyzed using a scanning electron microscope. The surface roughness of the helical-milled holes was lower than that for holes produced by conventional drilling. Scanning electron microscope images provided insights into the interaction of the hole surface with the chips during the chip evacuation stage under different speeds and feed rates. The microhardness of the aluminum layers increased after processing holes using drilling and helical milling operations. The axial feed/axial pitch had minimal influence on the microhardness increase in comparison to the cutting speed.

Keywords: fiber metal laminate; drilling; helical milling; surface roughness; damage; temperature; force



Citation: Bolar, G.; Dinesh, A.A.; Polishetty, A.; Shetty, R.; Hiremath, A.; Neelakantha, V.L. Performance Analysis of Helical Milling and Drilling Operations While Machining Carbon Fiber-Reinforced Aluminum Laminates. *J. Manuf. Mater. Process.* **2024**, *8*, 113. <https://doi.org/10.3390/jmmp8030113>

Academic Editors: Patricia Krawczak and Ludwig Cardon

Received: 17 April 2024

Revised: 13 May 2024

Accepted: 26 May 2024

Published: 29 May 2024



Copyright: © 2024 by the authors. Licensee MDPI, Basel, Switzerland. This article is an open access article distributed under the terms and conditions of the Creative Commons Attribution (CC BY) license (<https://creativecommons.org/licenses/by/4.0/>).

1. Introduction

The need for lightweight, high-performance materials in the automotive and aerospace industries has led to an increased demand for new-age composite materials that amalgamate the merits of metals and composite materials. The emergence of Fiber Metal Laminates (FMLs) is a response to these intricate demands. They consist of Fiber Reinforced Polymers (FRPs) sandwiched between thin metal/alloy sheets, combining the strength of metals/alloys with the exceptional strength-to-weight ratio of FRPs. Presently, the skin panel of the upper fuselage of the aircraft is being built primarily by the use of FMLs [1].

Generally, FMLs are identified based on the FRPs used or on the type of metal used [2–4]. Based on the used metal/alloy sheets, the most widely used FMLs are aramid-reinforced aluminum laminate (ARALL), carbon fiber-reinforced aluminum laminates (CARALL), and glass-reinforced aluminum reinforced epoxy (GLARE) [5,6]. Identification of FMLs is also conducted based on the positioning of the metal layers within the multi-layer configuration, wherein the metal layers can be placed internally or externally during stacking. Another way in which the FMLs are identified is based on the direction of the fibers in the FRPs as unidirectional or cross-ply FMLs [7].

Even though FMLs are processed as near-net-shape structures, almost all practical applications require the fastening of FMLs during assembly, either through mechanical fasteners or adhesive bonding [8]. To date, mechanical fasteners that include temporary fasteners such as bolts or permanent fasteners like rivets [9] are the preferred joining method, as such methods do not require additional surface preparation and ease of disassembly during inspection [10]. In both cases, FMLs are subjected to secondary operations such as drilling to make holes within the FML structure. It is reported that the number of holes drilled for commercial aircraft assembly varies between 1.5 million and 3 million [11,12]. For the reliable functioning of the assembled part, it is imperative to produce superior surface quality holes, which will result in the mitigation of structural failure due to stress and fatigue. Almost all aircraft industries impose stringent norms, facilitating the requirement of a smooth surface finish of the drilled holes to reduce catastrophic failure when the aircraft is in operation. For commercial aircraft, the drilled holes in composites are mandated to be burr- and scratch-free and should have a surface roughness value that is less than $3.2\ \mu\text{m}$ [13]. As a difficult-to-cut material, producing smooth, defect-free holes in FMLs through conventional drilling is often challenging. The interfaces generated between the layers of metal and FRP lead to increased machining process complexity. Higher thrust forces during drilling cause delamination of the FMLs. In fact, as per the published reports, drilling-induced delamination is the source of 60% of rejections in the aircraft industry. Deterioration of surface integrity during the drilling of FMLs is also linked to the abrasive nature of the reinforced anisotropic fibers. Studies have highlighted that the holes drilled in FMLs are attributed to varying surface roughness throughout the hole depth [14]. Also, the surface roughness of the metal layer is different from the FRP layer. While drilling metal/FRP stacks, the chip arising out of the hole drilled in the metal layer has the tendency to scrape the hole drilled in the FRP. Accordingly, the surface roughness of the hole in the FRP layer deteriorates compared to that in the metal layer. Additionally, FMLs based on aluminum alloys such as CARALL, ARALL, and GLARE tend to produce an excessive built-up edge (BUE) on the drill tool, leading to a higher rate of tool life deterioration [15]. This results in inadequate chip evacuation, and the chips left behind tend to erode the fibers and metal surface, consequently diminishing the surface finish of drilled holes [16]. The careful selection of the type of machining operation and the machining parameters becomes crucial for determining the final hole quality [17,18]. Higher feed and spindle speeds are reported to positively affect the surface quality of the drilled hole [19]. Boughdiri et al. [20] reported that during the drilling of GLARE laminates, the production of continuous chips may hinder the hole surface quality due to the prolonged interaction of the chips with the composite layer. Hence, it is advisable to have smaller broken chips while drilling FMLs. Moreover, at feeds lower than $0.08\ \text{mm/rev}$, chips adhere to or entangle with the flutes of the drill tool, in turn deteriorating the hole quality.

Delamination failure is one of the main types of failure occurring while machining FMLs. Delamination while machining FMLs occurs when the cutting force exceeds the interlaminar strength [21]. Thus, keeping the cutting forces to a minimum during the machining of FML is always desirable. Costa et al. [22] highlighted that during the drilling of CARALL laminates, cutting forces increase in magnitude when the tool encounters the aluminum metal layer, which reduces considerably while cutting the FRP layer. The phenomenon is attributed to the brittle nature of the FRPs. Kayihan et al. [23] performed drilling operations on Al-Ti-Carbon Fiber Reinforced Polymer (CFRP) laminates with

different stacking orders and found that at higher speeds and lower feeds, the cutting forces are independent stacking sequences. Another important machining factor severely affecting the hole quality was the cutting temperature. It is found that higher cutting speeds in FMLs lead to accelerated tool wear [24] and resin burn-out [25], which in turn leads to fiber pull-out and also weakens the FRP and metal interfaces [26]. Thus, modern machining techniques make use of minimum quantity lubrication (MQL) and cryogenic liquid nitrogen to bring down the cutting zone temperature during the drilling of FMLs [27]. Studies have shown improvement in the accuracy of the drilled hole in FMLs when MQL and cryogenic cooling environments were used [28]. However, the use of such coolants leads to an increase in production costs. The operational difficulties involved in conventional drilling necessitate the requirement of an alternate machining process to produce accurate, good-quality holes in the FMLs.

Helical milling is one such machining technology that has been successfully employed to produce superior-quality holes in FMLs. This method of hole production has proven to mitigate the disadvantages involved in conventional drilling. Bolar et al. [29] reported that the holes produced in CARALL have minimum surface roughness and are characterized by smaller-sized burrs as opposed to the conventional drilling method. Ge et al. [30] highlighted that the fatigue life of Al 2024-T3/Ti-6Al-4V stacks with holes produced by helical milling improved two times in comparison to Al 2024-T3/Ti-6Al-4V stacks with holes produced by conventional drilling. Sun et al. [31] found in their study that helical milling of Ti/CFRP/Al stacks results in discontinuous chips, allowing for easy chip evacuation and improving the surface quality of the hole produced. Li et al. [32] reported an abrupt increase in axial force between layers as the tool transits from the CFRP layer to the aluminum metal layer, which results in burr formation at the interlayers. Accordingly, a tool microlifting technique was proposed to overcome the problem at the inter-layers of the CFRP/Al stacks. Jiaying et al. [33] deliberated on the influence of cooling on delamination during helical milling of CFRP/Ti-6Al-4V stacks. Helical milling under MQL and cryogenic cooling conditions results in smaller delamination with improved hole surface quality. Xu et al. [34] examined the surface quality of holes produced in CFRP/Ti6Al4V stacks and concluded that diamond-coated drills fare better than the tool coated with TiAlN. Boutrih et al. [35] emphasized that the drilling sequence has a bearing on hole quality while helical milling CFRP/Ti6Al4V stacks. Accordingly, hole quality was better when drilling Ti6Al4V/CFRP stacks in comparison to the CFRP/Ti6Al4V stack.

The literature review suggests that the helical milling process can be a preferred technology to produce superior-quality holes in hard-to-cut FML materials. A few studies have explored the machining performance of drilling and helical milling operations while machining CARALL and have analyzed the influence of process variables on cutting forces, machining temperature, surface roughness, and dimensional accuracies of the processed holes. In the machining of materials like FMLs, thrust force and machining temperature are very influential, as they affect the performance of stacked materials. Very high thrust loads and temperatures resulting from unoptimized process variable selection can lead to surface damage and, in some cases, result in the delamination of the stacked material. However, research highlighting the influence of the thrust load and machining temperature on the hole surface finish, surface damage, and microhardness subsurface damage is scant. Moreover, studies critically evaluating the surface integrity and surface damage in CARALL are limited. Therefore, the work will initially focus on evaluating the influence of process variables on the thrust load and machining temperatures while drilling and helical milling holes in CARALL. It will further explore the effect cutting force and temperatures have on surface integrity (surface roughness, surface damage, and microhardness) while drilling and helical milling holes in CARALL. Accordingly, the work aims to minimize critical damages like delamination and debonding generated during the drilling process and improve the surface quality of holes made in CARALL FMLs. The outcome of the work will provide academicians and industries with the framework to process defect-free holes in CARALL FMLs.

2. Materials and Methods

The machining experiments were conducted on CARALL laminates. The laminates were fabricated by sandwiching strips of Al 2024-T3 with 0.5 mm thickness (supplied by Mangaldeep Metals and Alloys) and unidirectional carbon fiber prepreg (CFP) with 0.2 mm thickness (supplied by Bhor Chemicals). The layup procedure followed is depicted in Figure 1a. The CFP was manufactured using epoxy resin (A-45) and has a resin content of $38 \pm 3\%$ and a fiber density of 200 GSM. The mechanical properties of carbon fibers used in the CFP system and Al 2024-T3 alloy are provided in Table 1. The aluminum layers were subjected to sulfuric acid anodizing (SAA) to improve the corrosion resistance and interfacial bonding strength at the metal and FRP interface. Figure 1a shows the surface of the aluminum sheet, which shows the formation of nanopores as a result of SAA.

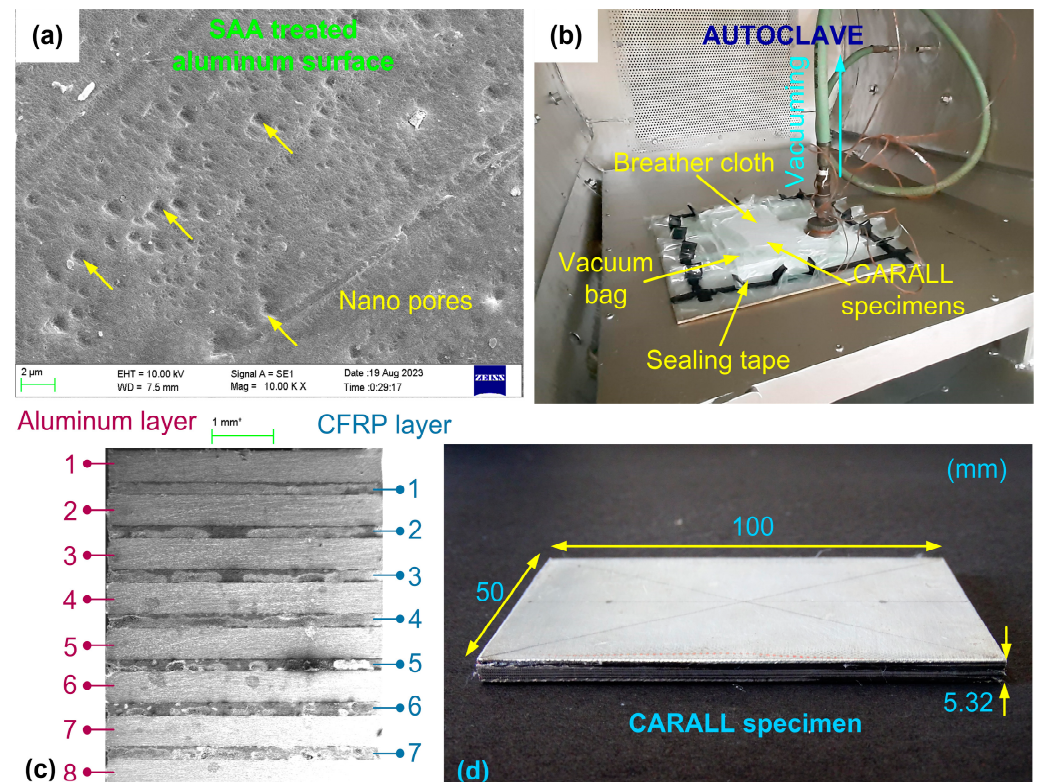


Figure 1. (a) Surface of aluminum sheet subjected to sulfuric acid anodizing; (b) specimen fabrication setup; (c) material stacking sequence; and (d) fabricated FML specimen.

Table 1. Mechanical properties of carbon fibers and 2024-T3 aluminum alloy.

	Carbon Fiber	Al2024-T3
Density (g/cm ³)	1.8	2.78
Filament diameter (μm)	7	-
Tensile strength (MPa)	4000	483
Tensile modulus (GPa)	240	73
Elongation (%)	1.7	18
Yield strength (MPa)	-	385
Shear strength (MPa)	-	283

The CARALL laminates were developed using the vacuum bagging method and autoclave cured using the setup shown in Figure 1b. The green FMLs were enclosed in a peel ply and kept on a mold plate. A breather cloth was placed above the peel ply to facilitate uniform vacuum pressure on the laminate. A sealant tape was used to prepare the vacuum bag, and the entire unit was then placed inside the autoclave for curing. A vacuum pump is used to evacuate the entrapped air from the vacuum bag.

Subsequently, the temperature of the autoclave was raised to 80 °C, with a consistent heating rate of 2 °C/min maintained for 30 min. In the second cycle, the temperature was elevated to 130 °C and sustained for 90 min. Throughout both cycles, the curing pressure remained at 6 bars. Figure 1c illustrates the stacking arrangement, while Figure 1d showcases the cured CARALL laminates. The holes were then drilled into the CARALL work specimens affixed to a vertical machining center (AMS Spark), utilizing the setup depicted in Figure 2a. Drilling and helical milling operations were performed using the tools shown in Figure 2b. For comparison between the drilling and helical milling operations, the holes were machined considering the parity between the machining times. Accordingly, selected process variables and the corresponding machining times are listed in Table 2.

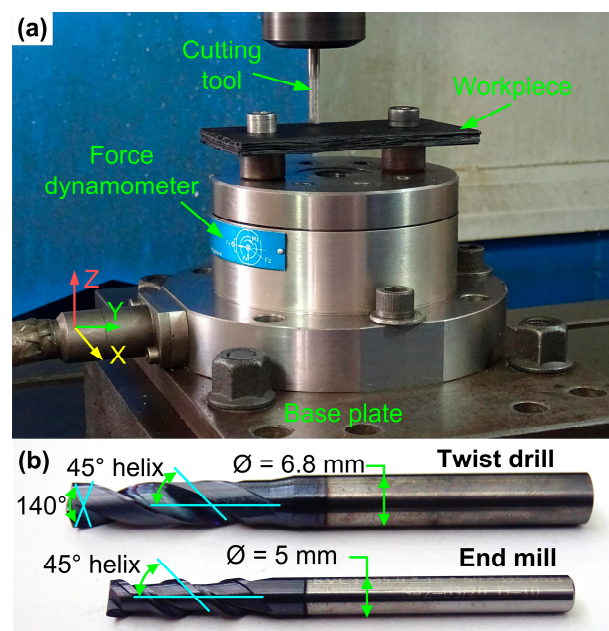


Figure 2. (a) Machining setup; (b) cutting tools for experimentation.

Table 2. Process variable combinations and corresponding machining time.

Case	Cutting Speed (V) (m/min)	Axial Feed (f_a) (mm/rev)		Tangential Feed (f_t) (mm/tooth)	Machining Time (t_m) (s)	
		Drilling	Helical Milling	Helical Milling	Drilling	Helical Milling
1	20	0.015	0.15	0.09	87	86
2	20	0.030	0.30	0.09	51	52
3	20	0.045	0.45	0.09	39	40
4	40	0.015	0.15	0.09	51	51
5	40	0.030	0.30	0.09	33	33
6	40	0.045	0.45	0.09	27	28
7	60	0.015	0.15	0.09	39	39
8	60	0.030	0.30	0.09	27	27
9	60	0.045	0.45	0.09	23	23

To measure the thrust force generated during machining, a dynamometer (Kistler 9272) connected to a charge amplifier (Kistler 5070A) and an analog-to-digital converter (type 5697A) are utilized, as depicted in Figure 3a. The force signal was acquired using Dynoware software (Type 2825D-02), and the sampling rate was set at 1000 Hz. Surface roughness was measured using a perthometer (Taylor Hobson—Form Talysurf 50) with a tip radius of 2.5 μm (see Figure 3b). The evaluation length of 3 mm was used, and the sampling length was chosen as 0.8 mm.

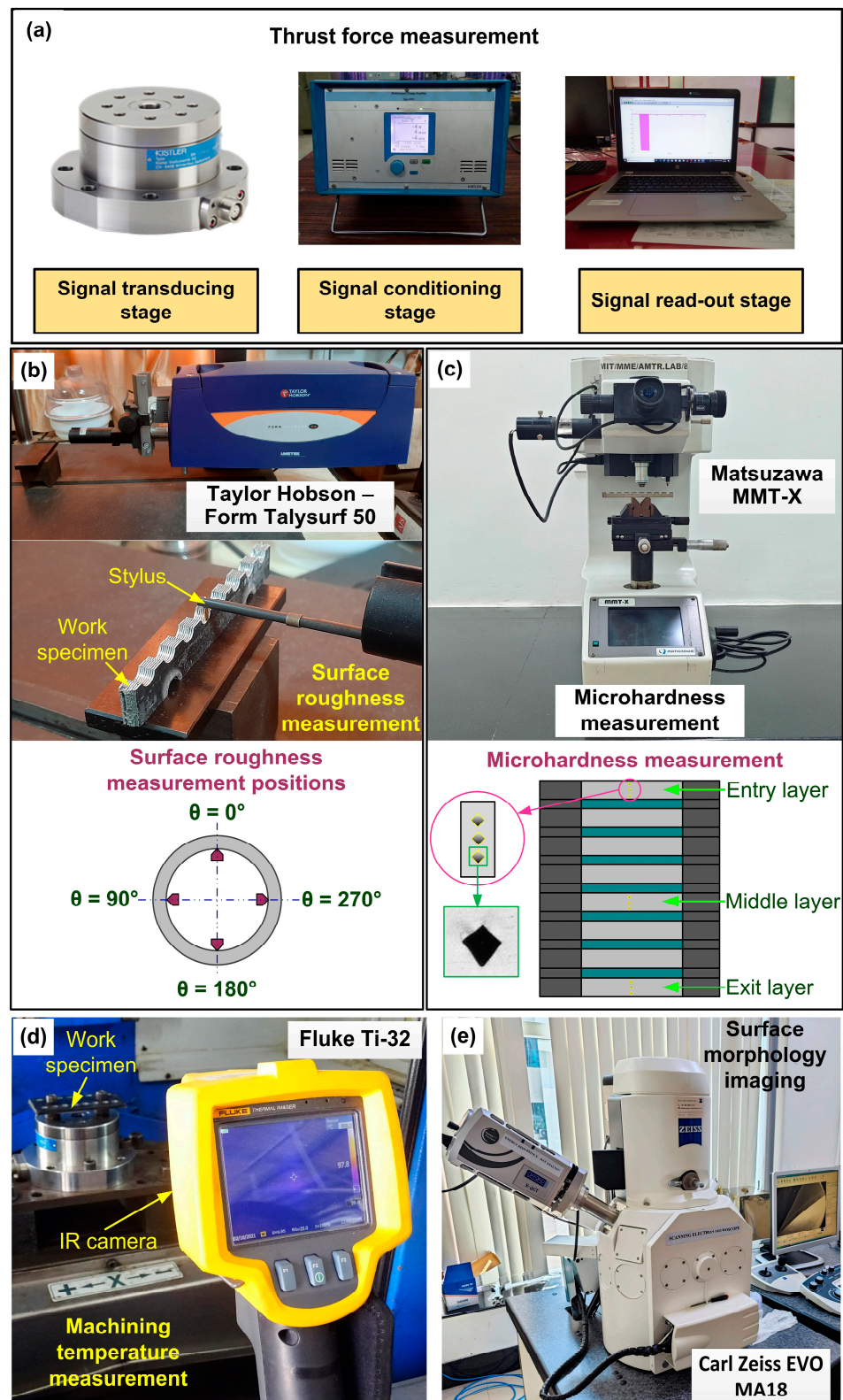


Figure 3. (a) Thrust force measurement; (b) surface roughness measurement; (c) microhardness measurement; (d) machining temperature measurement; (e) surface morphology imaging.

The rate of measurement was maintained at 0.5 mm/s, and the measurements were made at four locations. The microhardness measurements were taken at three different locations using the digital microhardness tester (Matsuzawa—MMT-X) with a diamond-shaped indenter by applying a 200 g load for 15 s, as shown in Figure 3c. The Fluke Ti32

infrared (IR) camera measured the machining temperature. The camera has a working range of 20 °C to 600 °C and an accuracy of ± 2 °C. For accurate measurement, the surface of the laminates was painted black, which possesses a thermal emissivity of 0.95. The IR camera was positioned at a distance of 0.1 m from the work material (see Figure 3d). The surface morphology of the machined hole was analyzed with the help of a Carl Zeiss EVO MA18 scanning electron microscope (SEM), as shown in Figure 3e.

3. Results and Discussion

3.1. Thrust Force

Thrust force is a significant factor when machining materials like CARALL. A very high thrust load can influence the surface roughness, burr size, and geometric accuracy of the holes. It can also initiate damages like fiber breakage and microcracking and result in the delamination of stacks. Such damages can render the FML useless or lower its service life [20,21]. Therefore, the thrust force behavior of the two hole-making operations was investigated. Figure 4a displays the effect the cutting speed employed during drilling has on thrust force. Thrust force was reduced as higher cutting speeds were selected. For example, for a fixed axial feed of 0.015 mm/rev, a thrust force of magnitude 180.6 N was measured when a speed of 20 m/min was selected. With 40 m/min employment, thrust force reduced to 164.6 N, indicating an 8.9% decrease as cutting speed increased. A favorable lower thrust force of 145.2 N was noted when holes were drilled with a 60 m/min cutting speed, showing a further 11.8% fall in the force magnitude. The aluminum alloy is plastically deformed during the machining process, thereby releasing energy in the form of heat. With higher cutting speeds, the rate of shear deformation increases, thus increasing the energy dissipation and the heat. At higher temperatures, the material yield strength is lowered, thus lowering the resistance to shearing and reducing the thrust load. Moreover, the polymer resin is softened at higher temperatures, easing the cutting process and reducing the thrust force [20,29]. Figure 4a also depicts the thrust force vs. axial feed plot for the drilling process. Thrust force increased with the selection of a higher feed. For a fixed speed of 20 m/min, an average thrust load of 180.6 N was measured while drilling with a feed of 0.015 mm/rev. At a feed of 0.03 mm/rev, the force increased to 189.7 N. Finally, when the axial feed is at its highest (0.045 mm/rev), the thrust force of 212.5 N is recorded. In this particular case, an increase in feed value from 0.015 mm/rev to 0.045 mm/rev led to a 17.7% increase in thrust force. As axial feed increases, uncut chip thickness also increases. In such a situation, the resistance offered by the chip increases, and more energy is required to shear the material. Due to this, there is an increment in the thrust load as the axial feed increases. Additionally, the hardened FRPs offer higher resistance during cutting, leading to an increased thrust force [36].

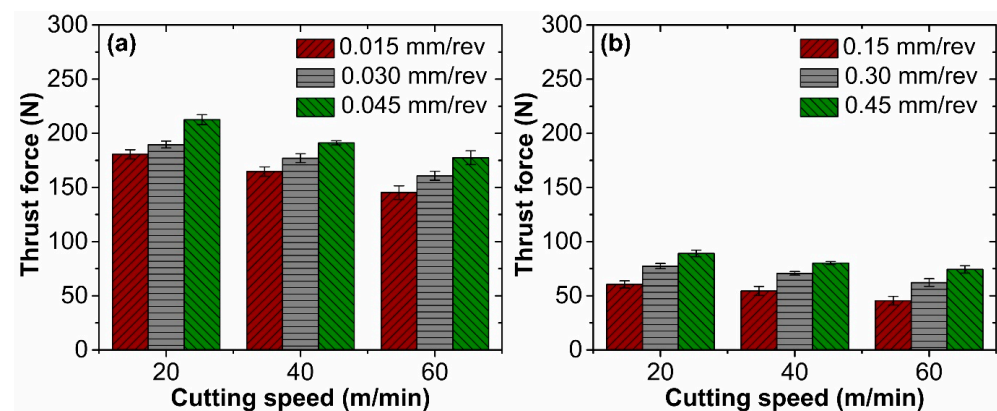


Figure 4. Thrust force variation with process variables in (a) drilling and (b) helical milling.

Thrust force fluctuation with the process variables during helical milling was similar to the trend observed during drilling. Thrust force is reduced with the increase in cutting

speed, as seen in Figure 4b. At a feed of 0.15 mm/rev, the thrust force of 60.6 N was measured when the cutting speed was held at 20 m/min. At a speed of 40 m/min, the thrust force was reduced to 54.4 N. At the highest selected cutting speed of 60 m/min, a thrust force of 45.5 N was registered. A decrease of 24.9% in force magnitude was recorded as cutting speed escalated from 20 m/min to 60 m/min. Similar to the drilling operation, at higher cutting speeds, the rate of shear deformation increases, thus increasing the energy dissipation and the heat. At such high temperatures, the yield strength of the material reduces, thus lowering the resistance to shearing and reducing the thrust load [37]. The impact of axial feed on thrust force is visualized in Figure 4b. Thrust force increased as higher levels of axial feed were selected. With the use of a lower feed (0.15 mm/rev), the measured thrust force was 60.6 N. At an axial feed of 0.30 mm/rev, the thrust force rose to 77.4 N. At the highest selected axial speed of 0.45 mm/rev, a thrust force of 89.1 N was registered. Notably, there is a 35.1% increase in thrust force as axial feed increases from 0.15 mm/rev to 0.45 mm/rev. As axial feed increases, the thickness of uncut chips also increases. This necessitates applying higher energy for material shearing, thereby increasing the thrust force magnitude [38].

However, it is to be noted that the recorded thrust forces are significantly lower during helical milling. Figure 5 illustrates the force signals generated for drilling and helical milling processes at identical machining conditions (Case 3). The mean thrust force during drilling was 216.6 N, while an average thrust force of 92.5 N was recorded during helical milling. Reduced thrust load is attributed to the helical milling kinematics. Hole milling is carried out using an end milling cutter, where the cutting occurs at the frontal and peripheral cutting edges. Since the load is distributed between the two cutting edges, the thrust load is reduced compared to the drilling operation [29,39].

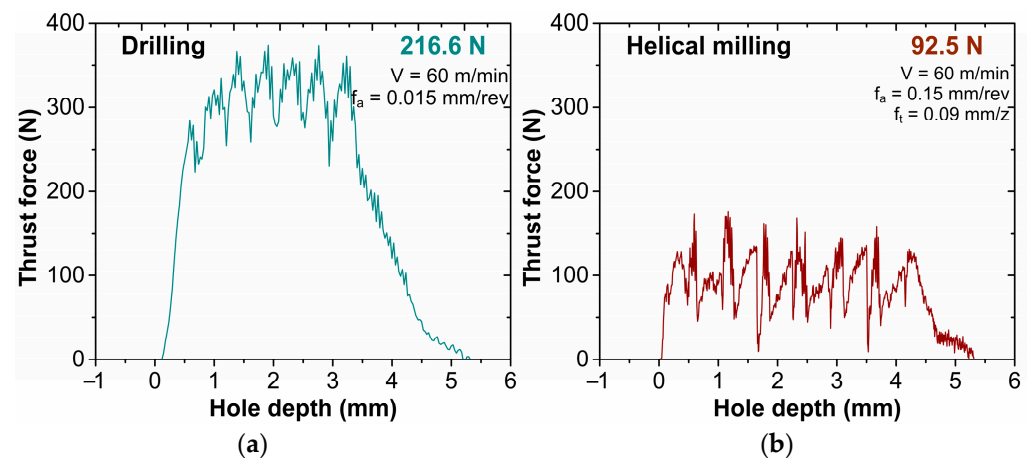


Figure 5. Raw force signal for (a) drilling and (b) helical milling.

3.2. Machining Temperature

The cutting temperatures attained while machining composites like FMLs are crucial as they influence the mechanical and failure behavior of the FMLs. Accordingly, the present work explores the development of machining temperatures under selected machining variables during the two hole-making operations. Figure 6a depicts how the machining temperature changes with the selected cutting speed and feed. At higher cutting speeds, the machining temperature increased. For instance, with a feed and speed held constant at 0.015 mm/rev and 20 m/min, respectively, a mean temperature of 100.5 °C was observed. However, when the speed increased to 40 m/min, an even higher temperature of 114.3 °C was registered. At the highest speed setting of 60 m/min, a mean temperature of 137.7 °C was observed. As noted, there was a 37.1% rise in cutting temperature when speed was raised from 20 m/min to 60 m/min. The rate at which the material deforms plastically increases at higher cutting speeds. In addition, the heat generated during the metal cutting will be concentrated at the cutting zone, thus increasing the magnitude of the measured

temperature [29]. The machining temperature was also affected by the selected axial feed. At a constant cutting speed of 20 m/min, using an axial feed rate of 0.015 mm/rev, the recorded mean temperature was 100.5 °C. With the increment in feed to 0.03 mm/rev, the temperature reduced to 97.2 °C. At the highest level of axial feed (0.045 mm/rev), the measured mean temperature was 93.4 °C. With the axial feed increment, a reducing temperature trend was observed. The mean temperature reduction with the axial feed increment is ascribed to the cutting time. Employment of higher axial feed reduced the cutting time. This reduces the work–tool contact and the time available for the heat to dissipate to the workpiece. The chip takes up a major part of the heat, which lowers the temperature at the cutting zone. Additionally, chip breakability improves at higher feeds. This helps reduce contact friction and the associated heat generation and temperature [40].

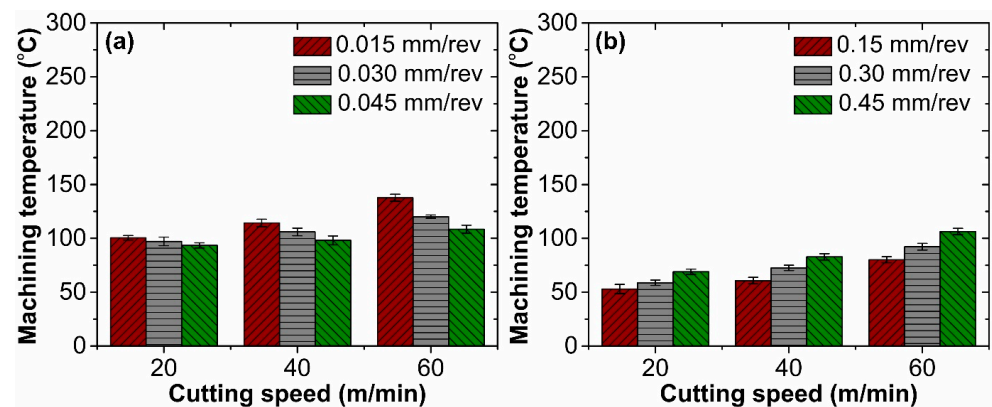


Figure 6. Machining temperature variation with process variables in (a) drilling and (b) helical milling.

Figure 6b shows the machining temperature variation with cutting speed during the helical milling process. When machining with a feed and speed of 0.15 mm/rev and 20 m/min, a mean cutting temperature of 52.9 °C was observed. At a speed of 40 m/min, an increased mean cutting temperature of 60.7 °C was recorded. Moreover, when the highest chosen speed of 60 m/min was applied, the temperature rose to 80.1 °C. Similar to the drilling process, the rate of material deformation increases as cutting speed increases. Consequently, heat generation and the machining temperature increase. Figure 6b also reveals the evolution of machining temperature with axial feed. In helical milling, with a machining speed of 20 m/min and a feed rate of 0.15 mm/revolution, a mean temperature of 52.9 °C was measured. When the feed rate was raised to 0.30 mm/revolution, the average machining temperature increased to 58.8 °C. Upon further increase to the highest axial feed level of 0.45 mm/revolution, the average temperature escalated to 68.9 °C. It is noteworthy that, in helical milling, the machining temperature rises in correlation with the axial feed increase. The trend is in contrast with that noticed during conventional drilling. Unlike drilling, helical milling is characterized by a higher work–tool contact. The end mill traverses a helical path and continuously interacts with the work material. Since the cutting occurs at the frontal and peripheral cutting edges, when the axial pitch is higher, the amount of material undergoing plastic deformation is significantly higher, thereby increasing the plastic deformation rate and the temperature [29].

When machining FMLs like CARALL, avoiding temperatures exceeding the glass transition temperature (T_g) and preventing thermal damage to the workpiece is preferable. In the present study, the selected process variables influence the heat generation rate and the magnitude of machining temperature in both hole-making operations. In the case of drilling, the maximum recorded temperature of 141.1 °C (Case 7) was higher than $T_g = 130$ °C for the epoxy resin used in the FMLs (see Figure 7). However, results show that helical milling for hole making was beneficial, as the recorded machining temperature of 82.7 °C was significantly lower than the T_g , indicating a lower probability of temperature-induced damages in CARALL.

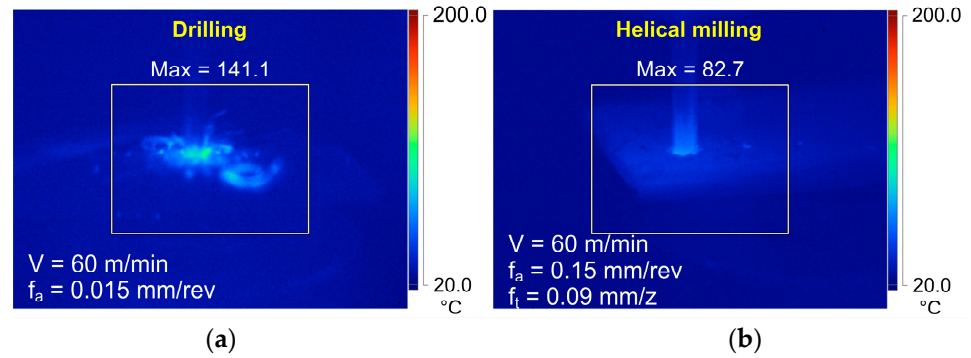


Figure 7. Comparison of machining temperature cartographs obtained for Case 7 during (a) drilling and (b) helical milling.

3.3. Surface Roughness

In the aerospace industry, the quality of the holes is essential, as it affects the functionality and service life of structural assemblies. Moreover, the choice of hole-making operations significantly affects the hole quality. Hence, an analysis of hole quality, specifically considering surface roughness, was conducted for the two hole-making operations utilized in this study. During drilling, variation in the surface roughness was observed for the selected speed and feed rates. Figure 8a presents the sway machining parameters that have surface roughness. As cutting speed increased, surface roughness decreased. At a constant feed of 0.015 mm/revolution, a mean roughness of 2.89 μm was observed when the speed was set at 20 m/min. At a 40 m/min cutting speed, a mean roughness of 2.65 μm was noted. At the highest employed speed of 60 m/min, the measured roughness was 2.25 μm . As observed, when the cutting speed increased to 40 m/min, the average surface roughness decreased by 8.3%. An increase in cutting speed to 60 m/min led to an additional reduction in measured surface roughness of 13.9%. The increase in surface roughness at reduced cutting speed can be attributed to chip size and built-up edge (BUE) formation [41]. Drilling at a lower cutting speed produces long, continuous chips. These work-hardened chips abrade the hole surface and erode the material from the CFRP layers as it evacuates through the tool flute [41]. Further, aluminum alloy tends to stick to the tool’s cutting edge when the cutting speeds are low. However, as the cutting speed increased, surface roughness reduced. The noted enhancement in surface finish is linked to the decrease in chip size and the elevated temperatures developed at higher cutting speeds. At higher cutting speeds, small-sized chips are produced, thereby reducing the intensity of scratches on the drilled holes’ surface. Higher cutting temperatures soften the resin material, smearing it across the machined surface and on top of the CFRP layers, generating a smoothing effect [29].

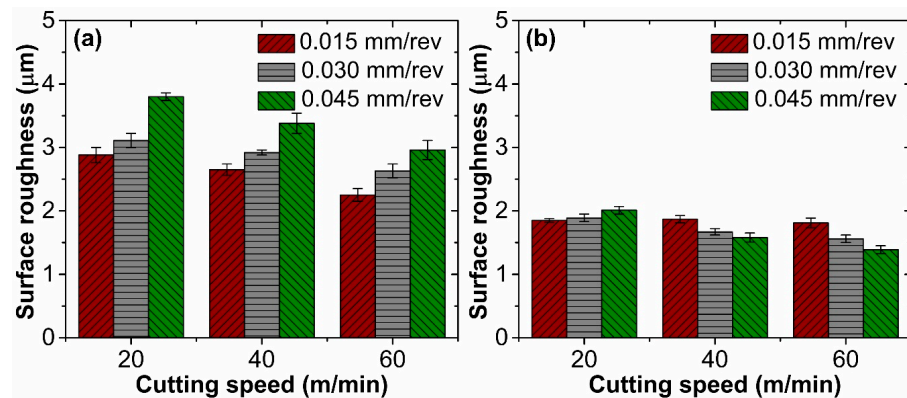


Figure 8. Surface roughness variation with process variables in (a) drilling and (b) helical milling.

Selected axial feed also affected the surface roughness in drilled holes. At a cutting speed of 20 m/min and a feed rate of 0.015 mm/rev, a mean roughness of 2.89 μm was

recorded. Further, at a feed of 0.03 mm/revolution, the measured mean roughness was 3.11 μm . When utilizing the highest feed of 0.045 mm/revolution, surface roughness was increased to 3.8 μm . At lower feeds, the drilled holes indicated the presence of feed marks. However, critical damages like fiber pull-out and breakage were not observed at lower feeds, thereby producing holes with better surface quality. However, at higher feeds, fibers were exposed due to increased thrust loads, and fiber pull-out (Figure 9) was noted under extreme conditions, deteriorating the surface quality.

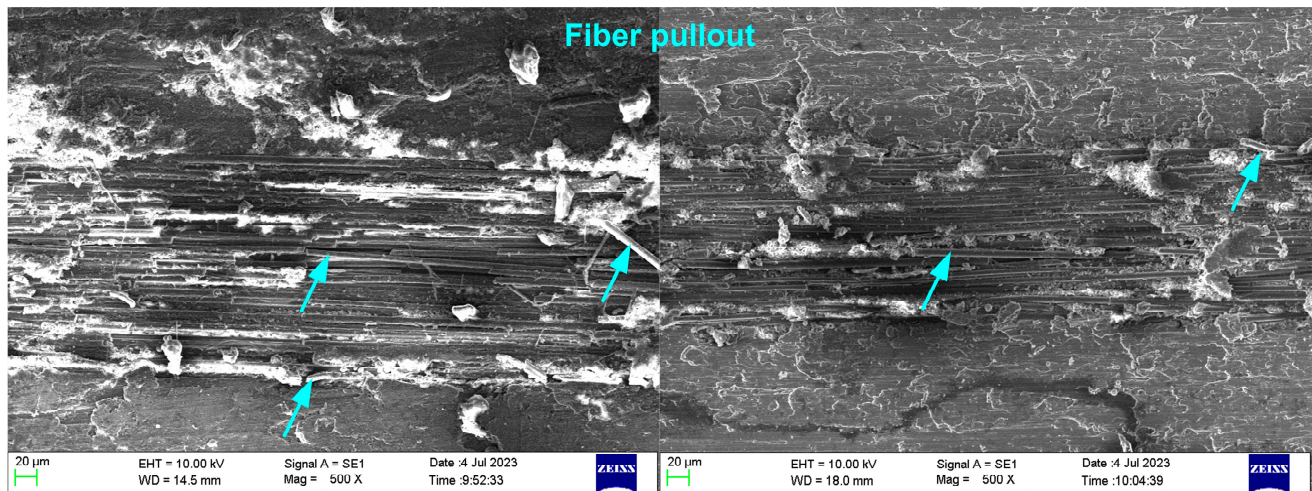


Figure 9. Fiber pull-out was observed at higher feed conditions during drilling.

Figure 8b shows the influence cutting variables have on surface roughness during helical milling. The surface roughness varied with cutting speed and axial feed. Milling with a lower feed, the axial feed, and the cutting speed interaction displayed a non-linear relationship. For a feed of 0.15 mm/rev, the mean surface roughness was 1.85 μm in holes cut at 20 m/min. When the cutting speed increased to 40 m/min, there was an increase in the mean roughness, which stood at 1.87 μm . A lower mean roughness of 1.81 μm was recorded with a 60 m/min speed. At a lower feed of 0.15 mm/rev, higher roughness at a smaller cutting speed is attributed to BUE formation and a higher force magnitude. BUE adhered to the bore surface, thereby deteriorating the surface quality. Also, material plowing was noted at the lower axial pitch, which generated feed marks. Additionally, due to the higher thrust load, carbon fibers in helical-milled holes were subjected to bending and eventual peeling. As a result, the CFRP layer exhibited poor surface quality, thus increasing the surface roughness of the FML as a whole [27]. However, at the higher selected cutting speed, the softened matrix material showed signs of smearing over the machined hole surface, thus reducing the surface unevenness and improving the surface finish.

However, with higher speeds of 40 m/min and 60 m/min, mean surface roughness decreased as the axial pitch increased. For example, for a 40 m/min cutting speed, a mean roughness of 1.87 μm was recorded when the axial pitch of 0.15 mm/rev was utilized. At a feed of 0.30 mm/rev, a mean roughness of 1.67 μm was recorded. Further, a 0.45 mm/rev feed helped produce surfaces with a mean roughness of 1.58 μm . A similar trend was obtained for a cutting speed of 60 m/min. Diminished surface finish at lower feed is ascribed to the formation of feed marks. Material removal resulted in material plowing and non-uniform plastic deformation at a lower pitch, producing feed marks on the machined surface. Additionally, the CFRP layers showed signs of fiber peeling and void formation, thereby increasing the roughness of the hole surface. However, the adaptation of a higher axial pitch produced defect-free surfaces, thus improving the machined surface quality. The resin material that underwent plasticization smeared and occupied the gaps available at the CFRP layers, thereby closing the gaps and improving the surface finish.

Closer observation reveals that the surface of the holes produced by milling operations showed an improved surface finish compared to the drilled ones (see Figure 10). Moreover, the magnitude of surface roughness of all the helical milled holes was considerably lower than the surface roughness requirements set by SANDVIK (less than $3.2\ \mu\text{m}$) [42], indicating the helical mill operation's capability to produce excellent-quality holes.

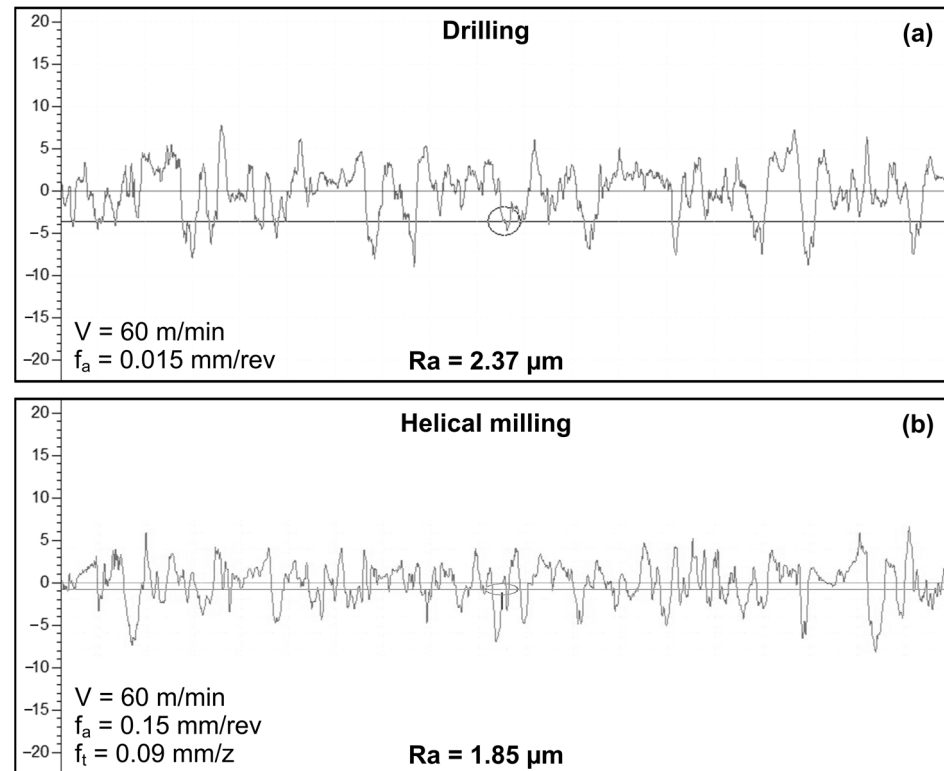


Figure 10. Comparison of surface roughness profiles obtained for Case 7 during (a) drilling and (b) helical milling.

3.4. Surface Morphology

The selected hole-making operations influence the hole quality. Figure 11 depicts the various forms of damage observed during the drilling process. The hole surface indicated the existence of deep groove marks created by strain-hardened continuous chips produced during the drilling operation at lower cutting speeds and feed conditions (see Figure 11a). The chips also interacted with the CFRP layer, resulting in material erosion. Moreover, fiber shearing, breakage, and fiber pull-out were noted in holes drilled at lower cutting speeds and higher feed conditions (see Figure 11b). Such damages result from the higher thrust force and temperatures [27]. Feed marks were observed on the hole surface drilled with lower axial feed (see Figure 11c). The hole surface showed signs of material smearing at higher cutting speeds during the drilling operation (see Figure 11d). As cutting speed increased during drilling, machining temperature also escalated. At higher temperatures, the resin material underwent thermal softening, smearing the material against the machined hole wall and improving the surface finish. Waste material ingress and interlayer burr formation are observed in the drill holes, as seen in Figure 11e. The selected feed influenced the surface finish of drilled holes. Moreover, adhered debris was commonly observed on the surface of the drilled holes (Figure 11f). As observed, the holes produced by drilling showed signs of surface anomalies in the form of feed marks, material smearing, fiber bundle exposure, and fiber pull-out, mostly attributed to the high thrust force and machining temperatures. Since helical milling aided in lowering thrust force and temperatures, the quality of milled holes was also studied to identify the presence of any surface irregularities [29].

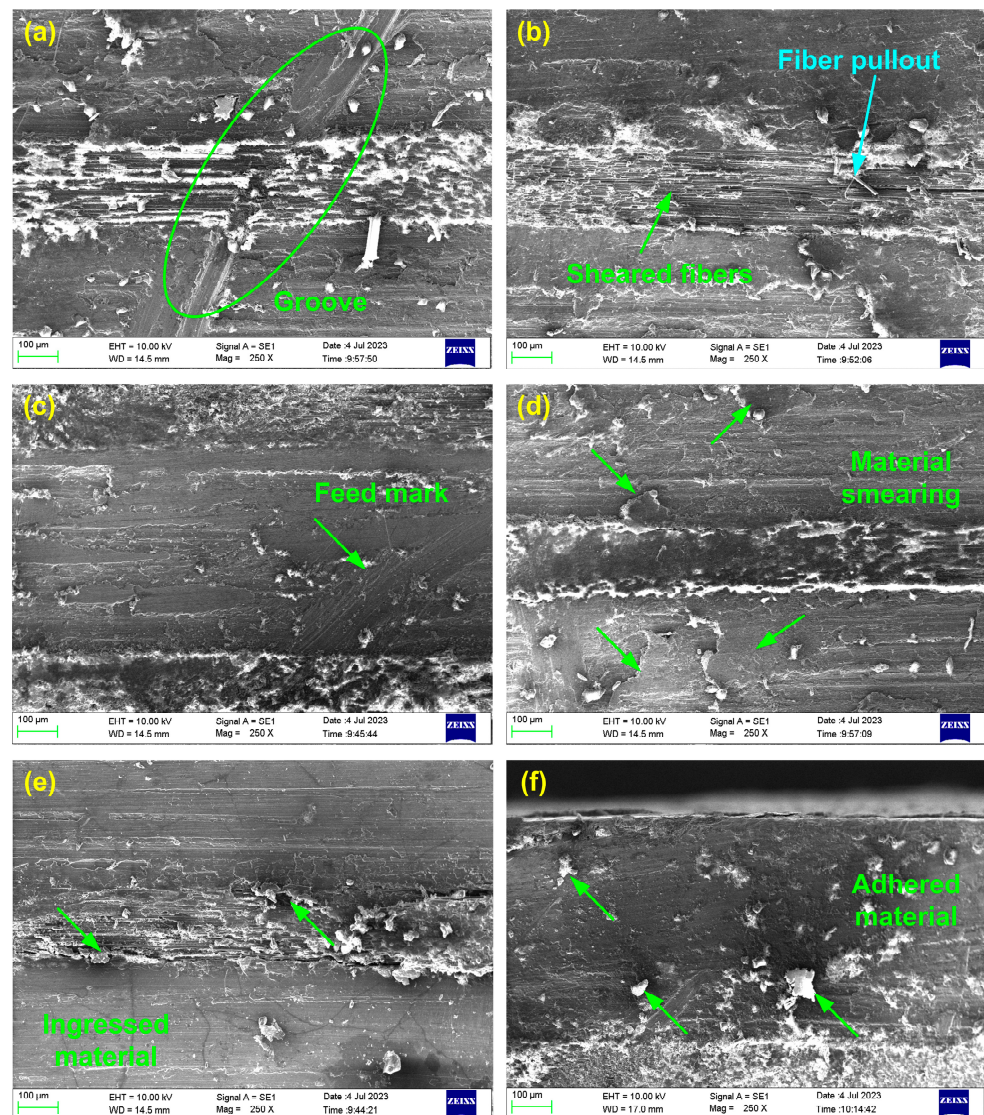


Figure 11. Surface damages in the form of (a) grooves, (b) fiber pullout, (c) feed marks, (d) material smearing, (e) material ingestion, and (f) material adhesion were observed in the drilled holes.

The characterization of milled holes revealed the presence of chip debris adhering to the hole surface, as seen in Figure 12a. The kinematics of the helical milling operation produces broken, discontinuous chips. Due to their light weight and size, these chips find it challenging to extrude from the cutting area without cutting fluid, thus adhering to the wall of the milled hole. Material smearing was characterized by holes machined at higher cutting speed (see Figure 12b). The smearing is the result of high-temperature material softening occurring at higher cutting speeds [29]. Further inspection revealed the formation of feed marks on the metal surface (see Figure 12c). The feed marks were prominent in holes subjected to lower axial pitch cutting conditions. Feed mark formation is attributed to plowing action, which generates a non-uniform plastic flow of the material at the cutting edge. At lower axial pitch, the carbon fibers in helical milled holes were subjected to bending and eventual peeling, resulting from the advancement of the tool corner into the fiber bundle (see Figure 12d).

In general, hole drilling with low feed and higher speed generated a clean-cut surface (see Figure 13a). The phenomenon is credited to material smearing observed at such machining conditions, where the temperature is substantially higher than T_g . Under such conditions, the resin, which is in the plastic state, is recast on the hole surface, thereby improving the surface finish. However, in the case of helical milling, an adaptation of

higher cutting speed and axial pitch produced a defect-free surface, as seen in Figure 13b. Moreover, in comparison to the drilling operation, far less damage was noted in the helical-milled holes. The quality of the hole surface was superior to that of the drilled ones, indicating the better utility of helical milling for processing holes for FMLs.

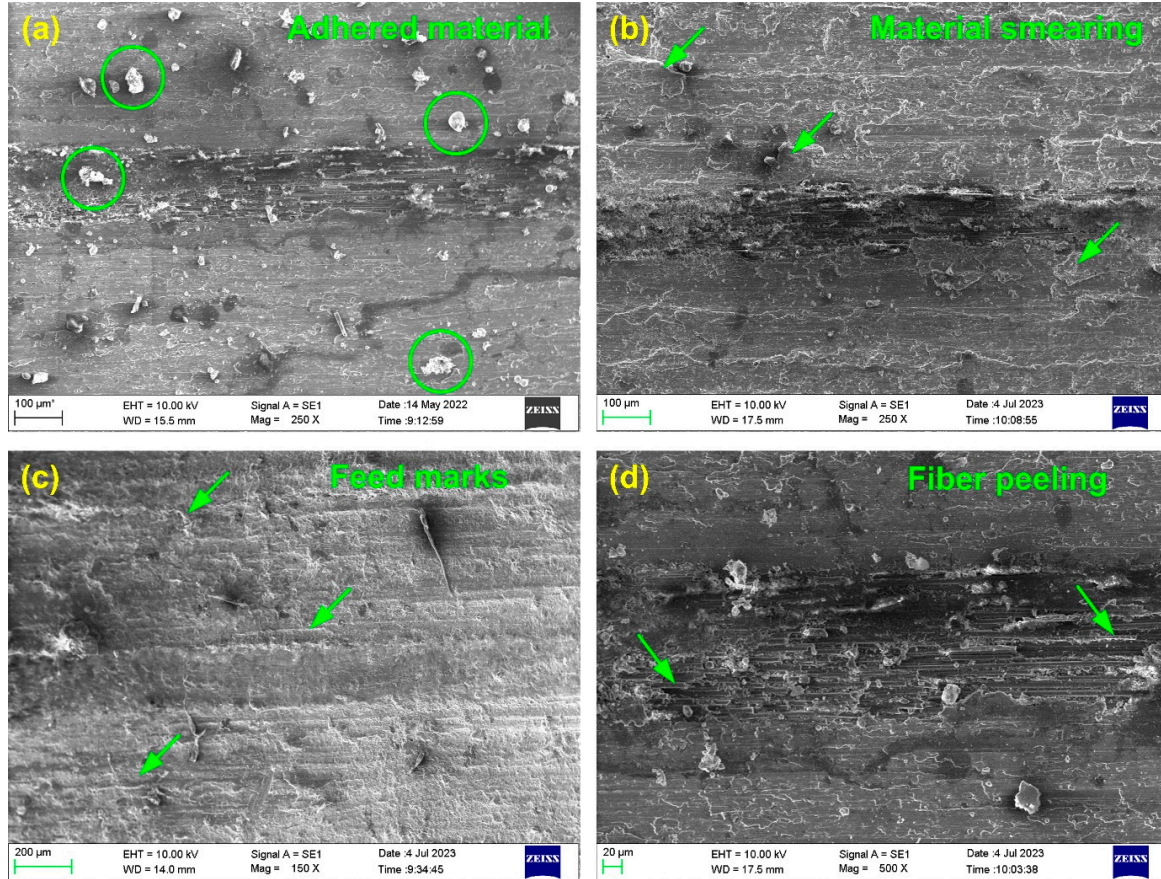


Figure 12. Surface damages in the form of (a) material adhesion, (b) material smearing, (c) feed marks, and (d) fiber peeling were observed in the helical milled holes.

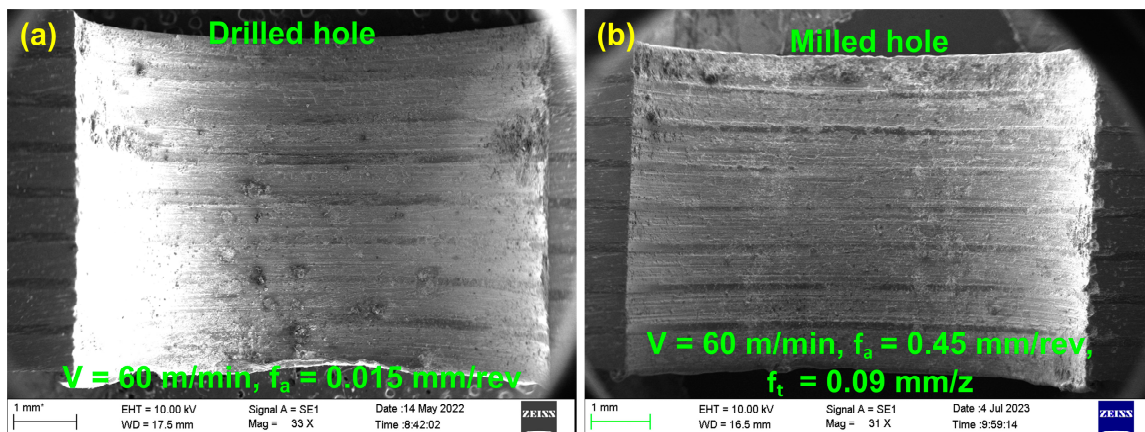


Figure 13. Holes with good surface finish were observed during (a) drilling and (b) helical milling.

3.5. Microhardness

The aluminum material is subjected to severe plastic deformation and temperatures during machining. Therefore, the microhardness of the holes processed using the drilling

and helical milling processes was measured and evaluated. For the drilled holes, microhardness ranged between 140.8 and 158.2 HV, showing a 7.3% to 20.5% increase compared to the bulk material microhardness of 131.2 HV. In the case of milled holes, microhardness ranged between 152.7 and 168.3 HV, displaying a 16.4% to 28.2% increase. As noted, the increase in microhardness during drilling is less than during the helical milling process. As the material is plastically deformed in the drilling operation, an enormous quantity of heat is generated, resulting in very high machining temperatures. As a result, the aluminum material is subjected to thermal softening, thus lowering its microhardness. However, machining temperatures are considerably lower in helical milling than in drilling, and the material dominantly exhibits strain hardening. The alterations in microstructure due to strain hardening increase the microhardness.

Additionally, the effect of process variables on microhardness during drilling and helical milling was investigated. Figures 14a and 15a display the effect the two process variables have on the microhardness of drilled and milled holes. The feed rate increase showcased the minimal influence of the microhardness variation. With the rise in drilling feed from 0.015 mm/rev to 0.045 mm/rev, a minor increment in the microhardness (3.1% to 4.9%) was noted. Similarly, in the case of helical milling, as the pitch increased from 0.15 mm/rev to 0.45 mm/rev, a 0.9% to 2.7% increase was noted. The increase in microhardness with axial feed and axial pitch is attributed to the higher work-hardening tendency of the material at higher axial feed. The microhardness displayed a decreasing trend with the cutting speed for both processes. As the cutting speed increased from 20 m/min to 60 m/min, the microhardness decreased by 3.9% to 6.3%. In the case of helical milling, a 3.1% to 4.7% decrease was measured. The reduction in microhardness with higher cutting speeds is attributed to the temperature-induced softening of the work material.

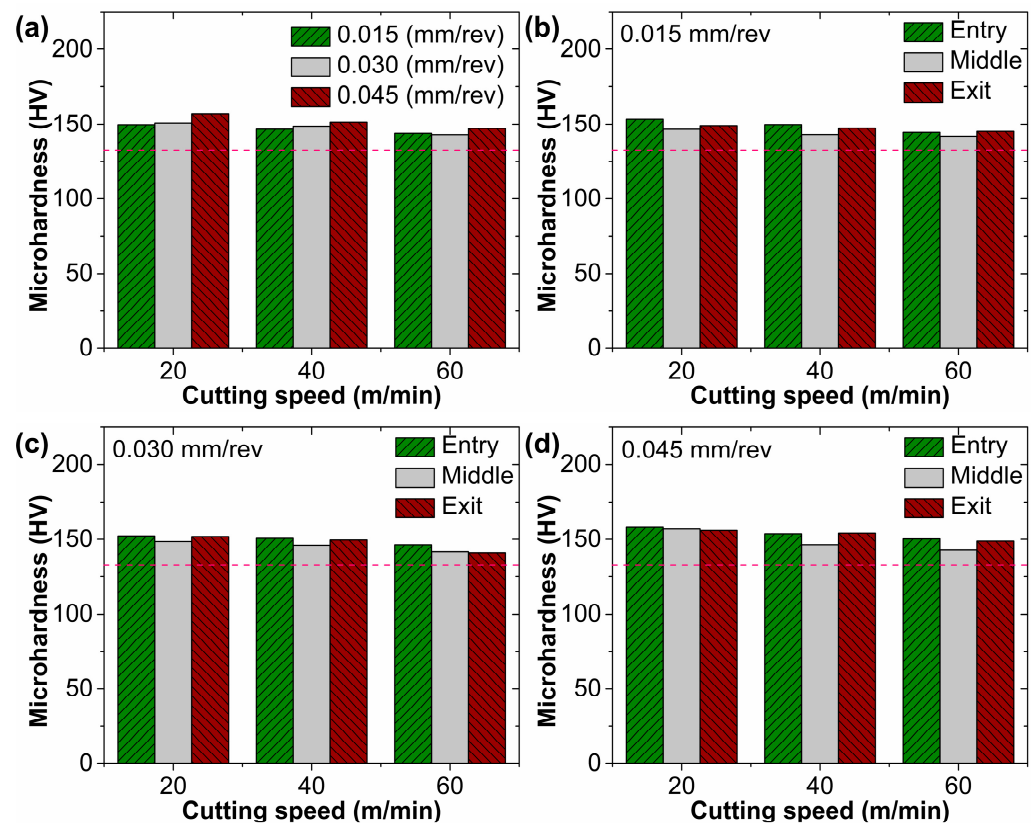


Figure 14. (a) Average microhardness vs. process variables for drilling operation; (b–d) microhardness at three different layers of the CARALL stack vs. process variables for drilling operation.

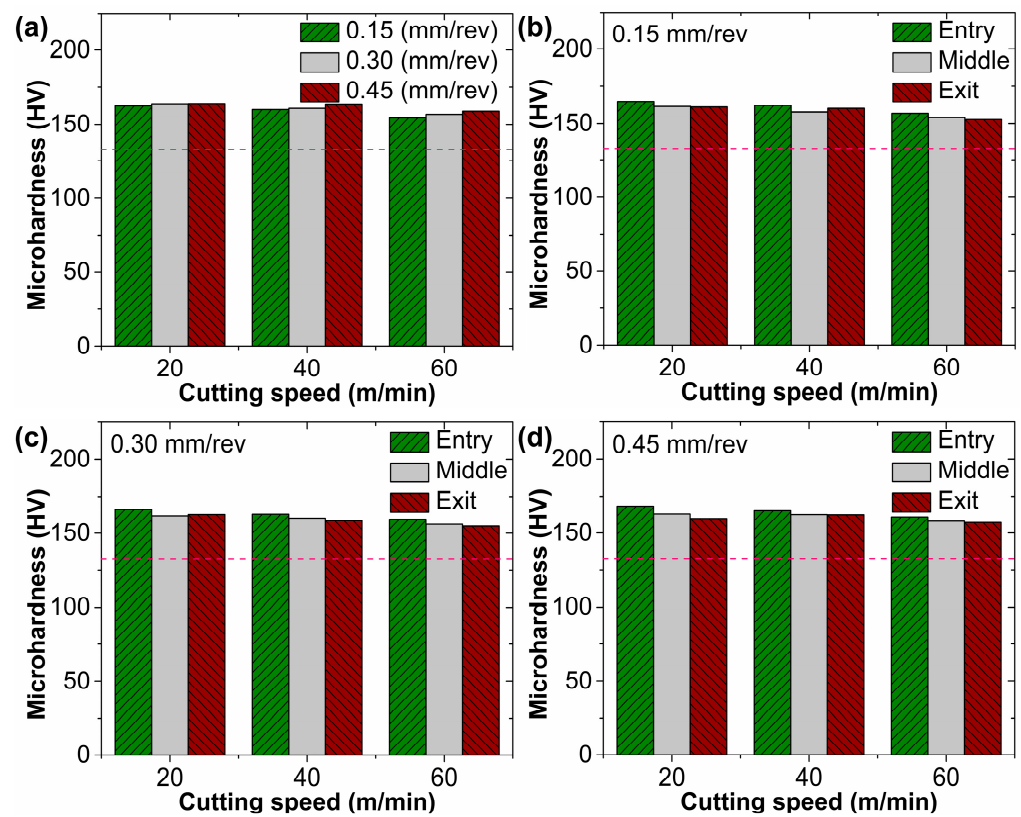


Figure 15. (a) Average microhardness vs. process variables for milling operation; (b–d) microhardness at three different layers of the CARALL stack vs. process variables for milling operation.

Furthermore, variation in the microhardness at three different layers was analyzed. In the case of drilling, the entry and exit layers exhibited similar microhardness values in the majority of the cases explored in the study. However, the microhardness at the middle layer of the CARALL stack was moderately lower compared to the extreme metal layers of the stack, as seen in Figure 14b,c. The variation in microhardness can be attributed to the machining temperatures the metal layers are subjected to during the drilling operation. The entry and exit layers are subjected to cutting temperatures. However, due to the higher thermal conductivity of the aluminum alloy, the heat is carried away, cooling the two outer layers quickly. However, the middle layer, which is subjected to cutting temperatures, cannot dissipate the heat quickly due to the surrounding epoxy, which has poor thermal conductivity. To some extent, the higher cutting temperatures during drilling soften the work material, thereby lowering its microhardness.

In most cases of helical milling operations (see Figure 15b,c), the microhardness was reduced at the exit layer compared to the entry and middle layers of the CARALL stack. In helical milling, at the entry layer, the material undergoes plastic deformation and work hardening, thus exhibiting higher microhardness. However, as the tool proceeds with the cutting and reaches the middle and exit layers, the frictional heat and the accumulated heat generated due to the plastic deformation can affect the microstructure, thus lowering the microhardness.

4. Conclusions

This work investigated the machining performance of helical milling and drilling operations while making holes in carbon fiber-reinforced aluminum laminates. The following important conclusions were noted:

- Thrust force increased with the axial feed, while a dropping trend was noted with increased cutting speed. The increase in thrust force with axial feed is attributed to the increase in uncut chip thickness, while the reduction in thrust force with cutting speed

is linked to material thermal softening. Moreover, the thrust force recorded during helical milling is 97–124 N lower than the conventionally drilled force magnitude. The decrease is attributed to load distribution at the frontal and peripheral cutting edges of the end mill, which differs from the drill tool, where cutting solely takes place at the frontal cutting edges.

- Selected process variables affect the machining temperature. A maximum temperature of 136.7 °C while drilling was recorded with a higher cutting speed of 60 m/min and a lower axial feed of 0.015 mm/rev. The maximum temperature observed in the drilling was higher than the glass transition temperature of epoxy resin. In the case of helical milling, a temperature of 80.1 °C was recorded for similar productivity conditions, indicating a lower probability of temperature-induced damages in the FML.
- The selected hole-making operation influenced the roughness of the holes. Higher surface roughness was recorded in holes processed using the drilling process. A maximum average roughness of 3.8 µm was noted during the drilling process, while a roughness of 2.01 µm was observed in helical milled holes, indicating the helical mill operation's capability to produce excellent-quality holes.
- The morphology of the drilled holes indicated the presence of defects such as grooves, feed marks, material smearing, material ingress, interlayer burr formation, fiber bundle exposure, and fiber pull-out. Helical-milled hole surfaces were characterized by the presence of smeared material, feed marks, and buckled fibers. Principally, in comparison to drilled holes, helical-milled holes exhibited better surface quality even under dry cutting conditions.
- The selected levels of process variables were conducive and favorable for carrying out drilling and helical milling operations without inducing any critical defects like delamination and debonding in CARALL FMLs.
- The microhardness of the aluminum layers increased by 7.3% to 20.5% in the case of drilling and by 16.4% to 28.2% in the case of helical milling. The axial feed/axial pitch had minimal influence on the microhardness increase in comparison to the cutting speed. The position of the aluminum layer in the CARALL stacking sequence, to some extent, influenced the post-machining microhardness.

Author Contributions: Conceptualization and methodology, G.B. and A.A.D.; formal analysis and investigation, A.P., G.B. and A.A.D.; resources, G.B.; data curation, A.A.D. and V.L.N.; writing—original draft preparation, G.B. and A.A.D.; visualization, A.H. and V.L.N.; writing—review and editing, A.P., A.H. and R.S.; supervision, G.B. and R.S. All authors have read and agreed to the published version of the manuscript.

Funding: This research received no external funding.

Data Availability Statement: All the data included in the manuscript can be provided by the corresponding author upon reasonable request.

Acknowledgments: We acknowledge the support provided by the Manipal Academy of Higher Education for carrying out the research work.

Conflicts of Interest: The authors declare no conflict of interest.

References

1. Ng, L.F.; Yahya, M.Y.; Leong, H.Y.; Parameswaranpillai, J.; Muthukumar, C.; Syed Hamzah, S.M.S.A.; Dhar Malingam, S. State-Of-The-Art Review on Developing Lightweight Fiber-Metal Laminates Based on Synthetic/Natural Fibers. *Polym. Compos.* **2023**, *44*, 6275–6303. [[CrossRef](#)]
2. Xie, M.; Zhan, L.; Ma, B.; Hui, S. Classification of Fiber Metal Laminates (Fmls), Adhesion Theories and Methods for Improving Interfacial Adhesion: A Review. *Thin-Walled Struct.* **2024**, *11*, 17–44. [[CrossRef](#)]
3. Mahesh, V.; Mahesh, V.; Harursampath, D. Ballistic Characterization of Fiber Elastomer Metal Laminate Composites and Effect of Positioning of Fiber Reinforced Elastomer. *Proc. Inst. Mech. Eng. Part L J. Mater. Des. Appl.* **2022**, *236*, 663–673. [[CrossRef](#)]
4. Taherzadeh-Fard, A.; Liaghat, G.; Ahmadi, H.; Razmkhah, O.; Charandabi, S.C.; Zarezadeh-Mehrizi, M.A.; Khodadadi, A. Experimental and Numerical Investigation of the Impact Response of Elastomer Layered Fiber Metal Laminates (Efmls). *Compos. Struct.* **2020**, *245*, 112–264. [[CrossRef](#)]

5. Seoane-Rivero, R.; Germán, L.; Santos, F.; Gondra, K. Development of New Hybrid Composites For High-Temperature Applications. *Polymers* **2023**, *15*, 4380. [[CrossRef](#)] [[PubMed](#)]
6. Costa, R.D.F.S.; Sales-Contini, R.C.M.; Silva, F.J.G.; Sebbe, N.; Jesus, A.M.P. A Critical Review on Fiber Metal Laminates (FML): From Manufacturing to Sustainable Processing. *Metals* **2023**, *13*, 638. [[CrossRef](#)]
7. Ghajar, R.; Ghadami, M. A Novel Experimental Method and Computational Micromechanical Model for In-Situ Damage Detection and Prediction of Stiffness Degradation In Cross-Ply FML. *Compos. Struct.* **2023**, *305*, 116–492. [[CrossRef](#)]
8. Ng, L.F.; Subramaniam, K. Composite Sandwich Panels with The Metallic Facesheets. In *Sandwich Composites*; CRC Press: Boca Raton, FL, USA, 2022; pp. 61–74.
9. Yang, Y.; Zhou, W.; Guo, Y.; Tong, Z.; Chen, L.; Ren, X.; Li, L. Effect of Laser Shock Peening without Protective Coating on Surface Integrity of Titanium-Based Carbon-Fibre/Epoxy Laminates. *Opt. Laser Technol.* **2023**, *167*, 109–685. [[CrossRef](#)]
10. Megahed, M.; Abd El-Baky, M.A.; Alsaedy, A.M.; Alshorbagy, A.E. Synthesis Effect of Nano-Fillers on the Damage Resistance of GLARE. *Fibers Polym.* **2021**, *22*, 1366–1377. [[CrossRef](#)]
11. Giasin, K.; Hawxwell, J.; Sinke, J.; Dhakal, H.; Köklü, U.; Brousseau, E. The Effect of Cutting Tool Coating on the Form and Dimensional Errors of Machined Holes in GLARE®Fibre Metal Laminates. *Int. J. Adv. Manuf. Technol.* **2020**, *107*, 2817–2832. [[CrossRef](#)]
12. Giasin, K.; Dad, A.; Brousseau, E.; Pimenov, D.; Mia, M.; Morkavuk, S.; Koklu, U. The Effects of through Tool Cryogenic Machining on the Hole Quality in GLARE®Fibre Metal Laminates. *J. Manuf. Process.* **2021**, *64*, 996–1012. [[CrossRef](#)]
13. Zhang, Q.; Zheng, S.; Yu, C.; Wang, Q.; Ke, Y. Digital Thread-Based Modeling of Digital Twin Framework for the Aircraft Assembly System. *J. Manuf. Syst.* **2022**, *65*, 406–420. [[CrossRef](#)]
14. Sui, S.; Song, G.; Sun, C.; Zhu, Z.; Guo, K.; Sun, J. Experimental Investigation on the Performance of Novel Double Cone Integrated Tool in One-Shot Drilling of Metal Stacks. *Int. J. Adv. Manuf. Technol.* **2020**, *109*, 523–534. [[CrossRef](#)]
15. De Melo Silva, W.; Martins, P.S.; De Carvalho, V.E.; Da Cruz, N.C.; Claudino, E.; Carneiro, J.R.G. Improving Precision in Aluminum Alloy Machining Due to the Application of Diamond-Like Carbon Thin Film. *J. Tribol.* **2021**, *143*, 71403. [[CrossRef](#)]
16. Dougan, M.A.; Yazman, S.; Gemi, L.; Yildiz, M.; Yapici, A. A Review on Drilling of FML Stacks with Conventional and Unconventional Processing Methods under Different Conditions. *Compos. Struct.* **2022**, *297*, 115913. [[CrossRef](#)]
17. Logesh, K.; Moshi, A.A.M.; Bharathi, S.R.S.; Hariharasakthisudhan, P. A Multi-Objective Grey Relational Approach and Regression Analysis on Optimization of Drilling Process Parameters for GLARE Fiber Metal Laminates. *Surf. Rev. Lett.* **2022**, *29*, 2250066. [[CrossRef](#)]
18. Kumar, D.; Gururaja, S.; Jawahir, I.S. Machinability and Surface Integrity of Adhesively Bonded Ti/CFRP/Ti Hybrid Composite Laminates under Dry and Cryogenic Conditions. *J. Manuf. Process.* **2020**, *58*, 1075–1087. [[CrossRef](#)]
19. Sridhar, A.K.; Bolar, G.; Padmaraj, N.H. Comprehensive Experimental Investigation on Drilling Multi-Material Carbon Fiber Reinforced Aluminium Laminates. *J. King Saud Univ. Sci.* **2022**, *34*, 391–401. [[CrossRef](#)]
20. Boughdiri, I.; Giasin, K.; Mabrouki, T.; Zitoune, R. Effect of Cutting Parameters on Thrust Force, Torque, Hole Quality and Dust Generation during Drilling of GLARE 2B Laminates. *Compos. Struct.* **2021**, *261*, 113562. [[CrossRef](#)]
21. Seif, A.; Fathy, A.; Megahed, A.A. Effect of Drilling Process Parameters on Bearing Strength of Glass Fiber/Aluminum Mesh Reinforced Epoxy Composites. *Sci. Rep.* **2023**, *13*, 12143. [[CrossRef](#)]
22. Costa, R.; Duro, J.N.S.; Sousa, V.F.C.; Silva, T.E.F.; Figueiredo, D.A.; Jesus, A.M.P. Drilling of CFRP/Al Multi-Material Stacks Using WC-Co CVD Diamond Coated Tools. *Procedia Struct. Integr.* **2024**, *53*, 376–385. [[CrossRef](#)]
23. Kayihan, M.; Karaguzel, U.; Bakkal, M. Experimental Analysis on Drilling of Al/Ti/CFRP Hybrid Composites. *Mater. Manuf. Process.* **2021**, *36*, 215–222. [[CrossRef](#)]
24. Sorrentino, L.; Turchetta, S.; Parodo, G. Drilling of Glare Laminates: Effect of Cutting Parameters on Process Forces and Temperatures. *Int. J. Adv. Manuf. Technol.* **2022**, *120*, 645–657. [[CrossRef](#)]
25. Parodo, G.; Rubino, F.; Sorrentino, L.; Turchetta, S. Temperature Analysis In Fiber Metal Laminates Drilling: Experimental and Numerical Results. *Polym. Compos.* **2022**, *43*, 7600–7615. [[CrossRef](#)]
26. Chen, X.; Zhao, W.; Zhao, G.; Jamil, M.; He, N. Tool Wear and Surface Quality during Milling CFRP Laminates under Dry and LN2-Based Cryogenic Conditions. *Int. J. Adv. Manuf. Technol.* **2022**, *123*, 1785–1797. [[CrossRef](#)]
27. Giasin, K.; Ayvar-Soberanis, S. Microstructural Investigation of Drilling Induced Damage in Fibre Metal Laminates Constituents. *Compos. Part A Appl. Sci. Manuf.* **2017**, *97*, 166–178. [[CrossRef](#)]
28. Giasin, K. The Effect of Drilling Parameters, Cooling Technology, and Fiber Orientation on Hole Perpendicularity Error in Fiber Metal Laminates. *Int. J. Adv. Manuf. Technol.* **2018**, *97*, 4081–4099. [[CrossRef](#)]
29. Bolar, G.; Sridhar, A.K.; Ranjan, A. Drilling and Helical Milling for Hole Making in Multi-Material Carbon Reinforced Aluminum Laminates. *Int. J. Light. Mater. Manuf.* **2022**, *5*, 113–125. [[CrossRef](#)]
30. Ge, J.; Feist, T.; Elmore, A.; Reji, R.; McLaughlin, B.; Jin, Y.; Sun, D. Open Hole Surface Integrity and Its Impact on Fatigue Performance of Al 2024-T3/Ti-6Al-4V Stacks. *Procedia CIRP* **2022**, *108*, 234–239. [[CrossRef](#)]
31. Sun, L.; Gao, H.; Wang, B.; Bao, Y.; Wang, M.; Ma, S. Mechanism of Reduction of Damage during Helical Milling of Titanium/CFRP/Aluminium Stacks. *Int. J. Adv. Manuf. Technol.* **2020**, *107*, 4741–4753. [[CrossRef](#)]
32. Li, X.; Jiao, A.; Liu, B.; Zhang, Y.; Liu, G.; Zhang, Z. Study on Helical Hole-Making Process of CFRP/Al Alloy Laminated Materials. *Int. J. Adv. Manuf. Technol.* **2022**, *121*, 6551–6568. [[CrossRef](#)]

33. Jiaying, G.E.; Guang, C.; Yongxiang, S.U.; Yunhe, Z.O.U.; Chengzu, R.E.N.; Xuda, Q.I.N.; Guofeng, W. Effect of Cooling Strategies on Performance and Mechanism of Helical Milling of CFRP/Ti-6Al-4 V Stacks. *Chinese J. Aeronaut.* **2022**, *35*, 388–403.
34. Xu, J.; Ji, M.; Chen, M.; El Mansori, M. Experimental Investigation on Drilling Machinability and Hole Quality of CFRP/Ti6Al4V Stacks under Different Cooling Conditions. *Int. J. Adv. Manuf. Technol.* **2020**, *109*, 1527–1539. [[CrossRef](#)]
35. Boutrih, L.; Makich, H.; Nouari, M.; Lanouar, B.E.N. Surface Quality In Dry Machining of CFRP Composite/Ti6Al4V Stack Laminate. *Procedia CIRP* **2022**, *108*, 758–763. [[CrossRef](#)]
36. Ramulu, M.; Branson, T.; Kim, D. A Study on the Drilling of Composite and Titanium Stacks. *Compos. Struct.* **2001**, *54*, 67–77. [[CrossRef](#)]
37. Sun, Y.; Sun, J.; Li, J.; Xiong, Q. An Experimental Investigation of the Influence of Cutting Parameters on Cutting Temperature in Milling Ti6Al4V by Applying Semi-Artificial Thermocouple. *Int. J. Adv. Manuf. Technol.* **2014**, *70*, 765–773. [[CrossRef](#)]
38. Giasin, K.; Barouni, A.; Dhakal, H.N.; Featherson, C.; Redouane, Z.; Morkavuk, S.; Koklu, U. Microstructural Investigation and Hole Quality Evaluation in S2/FM94 Glass-Fibre Composites under Dry and Cryogenic Conditions. *J. Reinf. Plast. Compos.* **2021**, *40*, 273–293. [[CrossRef](#)]
39. Amini, S.; Baraheni, M.; Hakimi, E. Enhancing Dimensional Accuracy and Surface Integrity by Helical Milling of Carbon Fiber Reinforced Polymers. *Int. J. Lightweight Mater. Manuf.* **2019**, *2*, 362–372. [[CrossRef](#)]
40. Zitoune, R.; Cadorin, N.; Collombet, F.; Šíma, M. Temperature and Wear Analysis in Function of the Cutting Tool Coating when Drilling of Composite Structure: In Situ Measurement by Optical Fiber. *Wear* **2017**, *376*, 1849–1858. [[CrossRef](#)]
41. Zitoune, R.; Krishnaraj, V.; Collombet, F. Study of Drilling of Composite Material and Aluminium Stack. *Compos. Struct.* **2010**, *92*, 1246–1255. [[CrossRef](#)]
42. Kumar, D.; Gururaja, S. Machining Damage and Surface Integrity Evaluation during Milling of UD-CFRP Laminates: Dry vs. Cryogenic. *Compos. Struct.* **2020**, *247*, 112–504. [[CrossRef](#)]

Disclaimer/Publisher’s Note: The statements, opinions and data contained in all publications are solely those of the individual author(s) and contributor(s) and not of MDPI and/or the editor(s). MDPI and/or the editor(s) disclaim responsibility for any injury to people or property resulting from any ideas, methods, instructions or products referred to in the content.